Trapping a Highly Reactive Nonheme Iron Intermediate That Oxygenates Strong C—H Bonds with Stereoretention

Joan Serrano-Plana,[†] Williamson N. Oloo,[‡] Laura Acosta-Rueda,[§] Katlyn K. Meier,[||] Begoña Verdejo,[⊥] Enrique García-España,[⊥] Manuel G. Basallote,*[,§] Eckard Münck,*[,||] Lawrence Que, Jr.,*[,‡] Anna Company,*[,†] and Miquel Costas*[,†]

[†]Grup de Química Bioinspirada, Supramolecular i Catàlisi (QBIS-CAT), Institut de Química Computacional i Catàlisi (IQCC), Departament de Química, Universitat de Girona, Campus de Montilivi, Girona E17071, Catalonia, Spain

[‡]Department of Chemistry and Center for Metals in Biocatalysis, University of Minnesota, Minneapolis, Minnesota 55455, United States

[§]Universidad de Cádiz, Facultad de Ciencias, Departamento de Ciencia de los Materiales e Ingeniería Metalúrgica y Química Inorgánica, Apdo. 40, Puerto Real, Cádiz 11510, Spain

[||]Department of Chemistry, Carnegie Mellon University, 4400 Fifth Avenue, Pittsburgh, Pennsylvania 15213, United States

[⊥]Instituto de Ciencia Molecular (ICMol), Universidad de Valencia, C/Catedrático José Beltrán, Paterna, Valencia 2 46980, Spain

S Supporting Information

ABSTRACT: An unprecedentedly reactive iron species (**2**) has been generated by reaction of excess peracetic acid with a mononuclear iron complex $[Fe^{II}(CF_3SO_3)_2(PyNMe_3)]$ (**1**) at cryogenic temperatures, and characterized spectroscopically. Compound **2** is kinetically competent for breaking strong C—H bonds of alkanes (BDE $\approx$ 100 kcal·mol^{-1}) through a hydrogen-atom transfer mechanism, and the transformations proceed with stereoretention and regioselectively, responding to bond strength, as well as to steric and polar effects. Bimolecular reaction rates are at least an order of magnitude

faster than those of the most reactive synthetic high-valent nonheme oxoiron species described to date. EPR studies in tandem with kinetic analysis show that the 490 nm chromophore of **2** is associated with two $S = 1/2$ species in rapid equilibrium. The minor component **2a** (~5% iron) has g-values at 2.20, 2.19, and 1.99 characteristic of a low-spin iron(III) center, and it is assigned as $[Fe^{III}(OOAc)(PyNMe_3)]^{2+}$, also by comparison with the EPR parameters of the structurally characterized hydroxamate analogue $[Fe^{III}(tBuCON(H)O)(PyNMe_3)]^{2+}$ (**4**). The major component **2b** (~40% iron, g-values = 2.07, 2.01, 1.95) has unusual EPR parameters, and it is proposed to be $[Fe^{V}(O)(OAc)(PyNMe_3)]^{2+}$, where the O—O bond in **2a** has been broken. Consistent with this assignment, **2b** undergoes exchange of its acetate ligand with CD_3CO_2D and very rapidly reacts with olefins to produce the corresponding cis-1,2-hydroxoacetate product. Therefore, this work constitutes the first example where a synthetic nonheme iron species responsible for stereospecific and site selective C—H hydroxylation is spectroscopically trapped, and its catalytic reactivity against C—H bonds can be directly interrogated by kinetic methods. The accumulated evidence indicates that **2** consists mainly of an extraordinarily reactive $[Fe^{V}(O)(OAc)(PyNMe_3)]^{2+}$ (**2b**) species capable of hydroxylating unactivated alkyl C—H bonds with stereoretention in a rapid and site-selective manner, and that exists in fast equilibrium with its $[Fe^{III}(OOAc)(PyNMe_3)]^{2+}$ precursor.
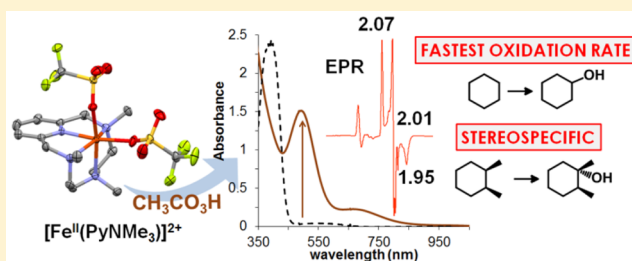
INTRODUCTION

The oxygenation of nonactivated alkyl C—H bonds is a very challenging reaction owing to their notorious chemically inert character. Consequently, highly reactive species are necessary to break these bonds.[1] However, because of their high reactivity, these species can only rarely be detected. In nature, C—H hydroxylation is mainly performed by iron-dependent enzymes, which create highly electrophilic species via finely controlled partial reduction of the O_2 molecule. Although it is now well established that the oxidation of C—H bonds can be carried out by oxoiron(IV) species generated in the catalytic cycles of both heme (e.g., cytochrome P450)[2,3] and nonheme

enzymes (e.g., α-ketoglutarate-dependent enzymes),[4,5] an Fe^{III}—OOH species has been observed and implicated as the C—H oxidizing species in the catalytic cycle of the antibiotic anticancer drug bleomycin, and in naphthalene dioxygenase, an enzyme that belongs to the Rieske oxygenase family.[6,7]

In parallel, biomimetic synthetic chemistry has produced a number of Fe^{III}—OOR (R = H, alkyl, acyl) compounds,[4,8] but not one has been shown capable of directly attacking strong alkyl C—H bonds.[9–12] Taking inspiration from nature, selected

nonheme iron complexes have been developed that elicit site-selective and stereoretentive C—H bond oxidation upon reaction with H_2O_2. Selectivity and stereospecificity exhibited by these catalysts provide strong support in favor of the intermediacy of metal-based oxidants akin to those involved with iron-dependent oxygenases. Presumably because of their high reactivity, these oxidants do not accumulate in solution, and it is challenging to establish their nature.

Herein we report the trapping and spectroscopic characterization of a metastable iron species that is kinetically and catalytically competent to attack strong alkane C—H bonds and can carry out this transformation at unprecedentedly fast reaction rates and with stereospecificity. This reagent also proves to be sensitive to the strength of the C—H bond, polar effects, and steric constraints, and therefore it bears the characteristics of a selective C—H hydroxylating agent. We propose this catalytically competent oxidant to be an $[Fe^V(O)(OAc)(L)]^{2+}$ species.

■ RESULTS AND DISCUSSION

Ferrous complex $[Fe^{II}(CF_3SO_3)_2(PyNMe_3)]$ (**1**) (Figure 1) was prepared and characterized in the solid state by X-ray
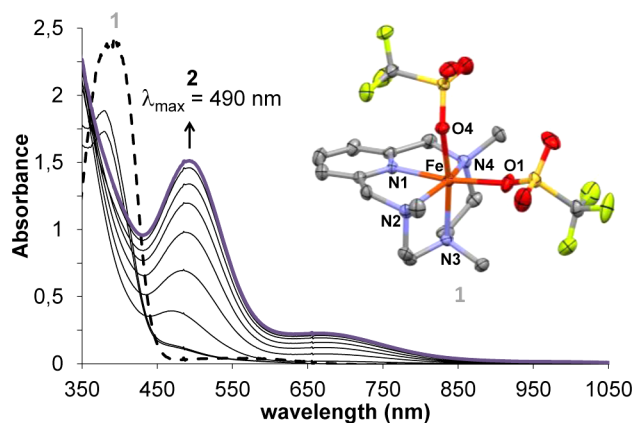
Figure 1. UV–vis spectra of **1** (1 mM, dashed line) and **2** (violet line). Solid black lines show the progressive formation of **2** upon addition of 4 equiv peracetic acid to **1** at −41 °C in acetonitrile over the course of 1 min. Inset: the thermal ellipsoid plot (50% probability) of $[Fe^{II}(CF_3SO_3)_2(PyNMe_3)]$ (**1**). Hydrogen atoms have been omitted for clarity.

crystallography and in solution by ^1H NMR spectroscopy (see the Supporting Information, SI, for details). X-ray analysis shows an octahedral ferrous center coordinated to the four nitrogen atoms of the macrocyclic ligand (PyNMe3) and to two triflates disposed *cis* to each other. The average Fe—N distance is 2.2 Å, indicating the presence of a high-spin iron(II) center.[13,14] The ^1H NMR spectrum of **1** in acetonitrile-d3 at 298 K reveals broad bands that span from 80 to −30 ppm, demonstrating that the iron center remains in the high-spin configuration ($S = 2$) in solution. This is further confirmed by a magnetic moment of 4.94 μ_B measured by the Evans' method. The basic chemical features of **1**, namely the presence of a tetradentate aminopyridine ligand with two *cis*-labile coordination sites, are the same as those of iron complexes with general formula $[Fe^{II}(^{N4}L)(X)_2]^{n+}$ (representative cases are $^{N4}L =$ BPMEN, BPMCN, TPA, PDP, PyTACN;[15] X = CH_3CN or CF_3SO_3) that mediate selective and stereoretentive C—H hydroxylation. While mechanistic studies on these catalysts

have implicated oxoiron(V) species as the oxidants responsible for their catalytic activity, the characterization of such species has remained elusive because they do not accumulate in solution.[16−19]

Treatment of **1** with 10 equiv peracetic acid (AcOOH) in the presence of excess cyclohexane at 25 °C under air resulted in the formation of cyclohexanol and cyclohexanone in a 5:1 ratio with a total turnover number of 9.5. Under analogous conditions, adamantane oxidation occurs with a high selectivity for the tertiary C—H site (normalized 3°/2° ratio = 23), while hydroxylation of the tertiary C—H bonds of *cis*-1,2-dimethylcyclohexane occurs with a high degree of stereo-retention (92%). The sum of these observations suggests that the combination of **1** and peracetic acid generates a metal-centered oxidant capable of attacking strong C—H bonds. Furthermore, the regio- and stereospecificity of the reactions excludes the involvement of unselective $HO^\bullet$ or related species and long-lived carbon-centered radicals.[20] To gain insight into the nature of the oxidant, we monitored the reaction of **1** with 4 equiv peracetic acid at −41 °C in acetonitrile by UV−vis spectroscopy and observed the rapid formation of a metastable brown species **2** ($t_{1/2} = 70$ s) with visible absorption features at 490 and 660 nm having a 7:1 relative absorbance ratio (Figure 1).

Kinetic Analysis of the Formation of 2 by Stopped-Flow UV−vis Spectroscopy. To get more information on the formation of intermediate **2**, detailed cryo-stopped-flow experiments were carried out using a diode-array detector. The reaction of **1** with peracetic acid in acetonitrile solution at −35 °C shows spectral changes that clearly reveal multiphasic kinetics in which intermediate **2** forms and then decays (Figures S6−S7). Global fitting analysis requires the involvement of another intermediate (**B**) preceding formation of **2** in order to obtain a satisfactory fit of the spectral changes, but **B** has no visible absorption (Figure S8). The kinetic model consists of three consecutive steps (**A → B → C → D**), where **A = 1**, **C = 2**, and **D** is the species formed upon decay of **2**.

Under pseudo-first order conditions of excess oxidant, the rate constant for the first resolved step (**A → B**) shows a linear dependence on the concentration of AcOOH (Figure S9), which yields a second order rate constant $k_{A→B} = 54 \pm 1$ M^{-1} s^{-1} at −35 °C. The appearance of a band at 330 nm and the absence of spectral features in the visible region suggest that this step consists of the oxidation of the starting complex to form an Fe^{III} species that corresponds to intermediate **B**. **B** then converts to **2** with a rate constant that does not show a clear dependence on the concentration of the oxidant ($k_{B→C} = 0.12 \pm 0.06$ s^{-1}). The large uncertainty associated with $k_{B→C}$ value is probably due to the existence of some parallel reaction of intermediate **B**, as revealed by the small deviation of the experimental kinetic traces at the absorption maximum of **2** from those expected for the 3-step kinetic model. Nevertheless, conversion of **B** to **2** requires the presence of more oxidant, as **2** does not form unless supra-stoichiometric amounts of AcOOH are added. The rate constant for the third step, which leads to decomposition of intermediate **2**, is also independent of the concentration of oxidant and shows a value of $k_{C→D} = 0.007 \pm 0.001$ s^{-1}.

Because peracetic acid solutions contain additional species (H_2O_2, acetic acid, water), it cannot be ruled out that some of the observed kinetic features may be caused by those additional species. To clarify this potential ambiguity, some kinetic experiments in acetonitrile solution were also carried out with

pernonanoic acid, which can be obtained as a pure solid. Reaction of **1** with 10 equiv of pernonanoic acid in acetonitrile at −35 °C produced a metastable species **2′** with analogous spectroscopic features as **2** (see SI for details). Again, an adequate fit of the spectral changes observed during the reaction of the starting complex **1** with the oxidant requires a model with three consecutive kinetic steps, the first one showing a second order rate constant of $k_{A \to B} = 11.9 \pm 0.6$ M^{-1} s^{-1} (Figure S13a) and the third one being independent of the concentration of pernonanoic acid, $k_{C \to D} = (2.3 \pm 0.3) \times 10^{-3}$ s^{-1}. Importantly, unlike with peracetic acid, the rate of the second step in this case does show a dependence on the concentration of the oxidant ($k_{B \to C} = 1.1 \pm 0.1$ M^{-1} s^{-1}, Figure S13b), supporting our suspicion that the second step in the peracetic acid reaction is complicated by one or more of the additional species present in solution. Importantly, the second order rate constants for the reactions of alkanes with **2** generated from either peracetic or pernonanoic acid are congruent.

Kinetic Analysis of the Reaction of 2 with Alkanes by Stopped-Flow UV–vis Spectroscopy. The decay of **2** is significantly accelerated by the addition of cyclohexane (Figure S14), requiring the use of stopped-flow UV–vis methods to follow the disappearance of **2** (490 nm) as a function of cyclohexane concentration (Figure 2a). The kinetic traces show
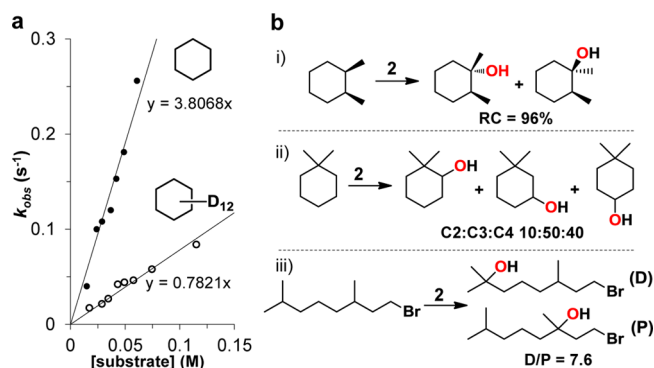

Figure 2. (a) Kinetic data for the reaction of **2** with cyclohexane at −35 °C (cyclohexane, filled circles; cyclohexane-d_{12}, open circles). (b) Reactivity of **2** with various substrates demonstrating its selectivity.

pseudo-first order behavior and can be fitted with single exponentials. The corresponding k_{obs} values are in turn found to be linearly dependent on substrate concentration (Figure 2a), affording a second order rate constant (k_2) of 2.8 ± 0.1 M^{-1} s^{-1} at −41 °C. Analysis of the reaction rates of **2** with cyclohexane as a function of temperature (Figure S15) reveal an activation barrier with a relatively small activation enthalpy ($\Delta H^{\ddagger} = 37 \pm 3$ KJ·mol^{-1}) and a negative activation entropy ($\Delta S^{\ddagger} = -76 \pm 8$ J·K^{-1}·mol^{-1}), consistent with a bimolecular reaction. Comparison of the k_2 values for substrates with weaker C—H bonds show an inverse correlation between the logarithms of second order kinetic constants (normalized by the number of equivalent C—H bonds that can be cleaved) versus BDE$_{C-H}$ (bond dissociation energy) of the weakest C—H bond of the hydrocarbon (Figure S18). *These results demonstrate that C—H bond cleavage by **2** is an important component of the rate-determining step and that even unactivated C—H bonds can be cleaved by **2** at fast reaction rates.*

Figure 2b shows that **2** exhibits significant selectivity in its reactions with various substrates. For the oxidation of

cyclohexane, cyclohexanol (**A**) and cyclohexanone (**K**) products were obtained with an A/K ratio of 4.5. In the case of adamantane, 1-adamantanol and 2-adamantanol/one were produced with a normalized 3°/2° selectivity of 29, while the hydroxylation of *cis*-1,2-dimethylcyclohexane to *trans*-1,2-dimethylcyclohexanol occurred with >95% retention of configuration. In addition, the oxidation of 1,1-dimethylcyclohexane yielded a mixture of C2, C3, and C4 alcohols and ketones in a relative ratio of 10:50:40, which showed that the sterically more congested C2 site was less prone to attack. Lastly, the hydroxylation of 1-bromo-3,7-dimethyloctane resulted in the preferential attack of the more electron-rich C7—H bond over the C3—H bond by a factor of 8. Taken together, these observations demonstrate a metal-based oxidant that discriminates among multiple C—H bonds based not only on the C—H bond strength but also on steric and polar factors.[21−26]

The significance of the ability of **2** to react with substrates having strong C—H bonds becomes more obvious when its reaction rates are compared with those determined for other iron-based oxidants. Thus far, hydroperoxoiron(III) species have only been shown capable of attacking weak C—H bonds such as those of xanthene.[11,27] Cleavage of much stronger C—H bonds such as those of cyclohexane has been described only for a few high-valent nonheme oxoiron complexes. Surprisingly, as shown in Figure 3 and Table 1, **2** is by far
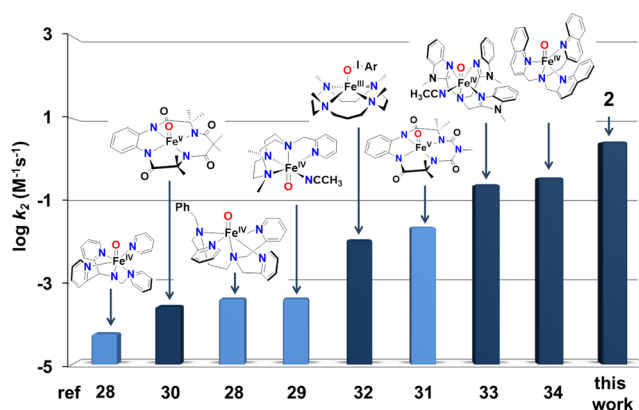
Figure 3. Cyclohexane oxidation rates (k_2) obtained at −40 or 25 °C for various nonheme iron complexes. Dark blue bars represent k_2 values at −40 °C, while light blue bars correspond to k_2 values at 25 °C.

the most reactive of such species. The reaction of **2** with cyclohexane at −41 °C is at least 4 orders of magnitude faster than several $S = 1$ oxoiron(IV) complexes.[28,29] Also, when compared to the two previously reported oxoiron(V) complexes supported by tetraamido macrocyclic ligands (TAML), the reaction rates for **2** are respectively 4 and 2 orders of magnitude faster,[30,31] even without correcting the 65-degree difference in temperature in the second case. Furthermore, **2** is more than 200 times more reactive than an iron(III)-iodosylarene adduct, which can be construed as a masked oxoiron(V) species.[32] The complexes that most closely approach **2** in C—H bond cleavage reactivity are the $S = 1$ complex [Fe^{IV}(O)(Me$_3$NTB)]$^{2+}$ (which is proposed to operate through a highly reactive high spin ($S = 2$) excited state) and the recently described $S = 2$ complex [Fe^{IV}(O)(TQA)-(NCMe)]$^{2+}$; both react with cyclohexane an order of

Table 1. Alkane Oxidation Reactions by Selected Non-Heme Iron High-Valent Species

high-valent species	k_2 (cyclohexane) (M^{-1} s^{-1}) (T)[a]	A/K[b] (cyclohexane)	KIE[c]	ref
2	2.8(1) (−40 °C)	1/0.2	5 (cyclohexane)	this work
[Fe^{IV}(O)(TQA)(NCMe)]$^{2+}$	0.37 (−40 °C)	0/0.35	25 (cyclohexane)	34
[Fe^{IV}(O)(Me$_3$NTB)]$^{2+}$	0.25 (−40 °C)		26 (PhEt)	33
Fe^{III}(13-TMC)/OIAr adduct	0.011 (−40 °C)	0.11/0.04	10 (cumene)	32
[Fe^{V}(O)(TAML)]$^{-}$	0.00026 (−40 °C)		26 (PhEt)	30
[Fe^{V}(O)(bTAML)]$^{-}$	0.023 (25 °C)	0.4/0.02	9 (PhCH$_3$)	31
[Fe^{IV}(O)(PyTACN)]$^{2+}$	0.0004 (25 °C)		27 (DHA)	29
[Fe^{IV}(O)(BnTPEN)]$^{2+}$	0.00039 (25 °C)	0.03/0.13	50 (PhEt)	28
[Fe^{IV}(O)(N4Py)]$^{2+}$	0.000055 (25 °C)	0.03/0.04	27 (PhEt)	28

[a]Second-order rate constant determined in cyclohexane oxidation. [b]Equivalents of cyclohexanol (A) and cyclohexanone (K) with respect to Fe obtained in the oxidation of cyclohexane. [c]KIE = kinetic isotope effect. Ligand abbreviations: TQA = tris(2-quinolylmethyl)amine; Me$_3$NTB = tris((N-methyl-benzimidazol-2-yl)methyl)amine; TAML = tetraamido macrocyclic ligand; bTAML = biuret tetraamidate macrocyclic ligand; 13-TMC = 1,4,7,10-tetramethyl-1,4,7,10-tetraazacyclotridecane; PyTACN = 1,4-dimethyl-7-(2-pyridylmethyl)-1,4,7-triazacyclononane; BnTPEN = N-benzyl-N,N′,N′-tris(2-pyridylmethyl)-1,2-diaminoethane; N4Py = N,N-bis(2-pyridylmethyl)-N-(bis-2-pyridylmethyl)amine.

magnitude more slowly than **2** (Table 1).[33,34] Thus, **2** is the most effective species observed to date in solution that can oxidize cyclohexane.

Intermediate **2** stands out from the other complexes in Figure 3 in yet another respect. As shown in Figure 2a, **2** oxidizes cyclohexane and cyclohexane-d_{12} at different rates, exhibiting a classical kinetic isotope effect (KIE) of **5**. This value is obtained as well from the product analysis of competitive oxidations of cyclohexane and cyclohexane-d_{12}, corroborating that **2** is in fact the actual C—H bond cleaving agent. In contrast, the other complexes in Figure 3 carry out C—H bond cleavage with large nonclassical KIE values. The subset consisting of the oxoiron(IV) complexes exhibits KIE values of 25−50 that have been attributed to H atom tunneling,[28,35] while the other subset comprising the two oxoiron(V) complexes and the iron(III)-iodosylarene adduct exhibit lower values of 9−26 (Table 1). As KIE values can depend on temperature and the nature of the substrate, the best comparison is for the oxidation of cyclohexane at −40 °C between **2** and [Fe^{IV}(O)(TQA)(NCMe)]$^{2+}$ where the KIE values differ by a factor of 5. What this difference tells us about the distinct natures of the oxidants and how they cleave C—H bonds remains to be uncovered, but it is clear that there is a difference. However, the classical KIE value of 5 found for **2** matches those found for nonheme-iron-catalyzed hydroxylation of cyclohexane by H$_2$O$_2$. For these catalysts, there is strong indirect evidence for an Fe^{V}(O) oxidant, but it has not yet been spectroscopically identified.[16,36] In at least three cases, evidence for the Fe^{V}(O) oxidant has been obtained in the gas phase by electrospray ionization mass spectrometry.[16,18,37] In a few cases, hydroperoxy- or acylperoxyiron(III) intermediates have been observed and spectroscopically characterized;[38−41] unlike **2**, these intermediates persist in a steady-state phase at −40 °C, during which oxidation products are formed catalytically. The decay occurs upon depletion of H$_2$O$_2$ at a rate independent of the nature of the substrate and its concentration. This kinetic behavior makes them precursors to the actual oxidant. In contrast, **2** is unique as the only catalytic intermediate shown to effect C—H bond cleavage directly.

EPR Insights into the Nature of 2. EPR spectroscopy turned out to be an excellent tool to characterize the nature of the iron center in **2**. We have studied a series of EPR samples prepared at −50 °C using a 1:3 (v/v) acetonitrile:acetone glassing solvent mixture.[42] This procedure yielded well resolved EPR features in the $g = 2$ region that could be monitored

concurrent with the growth and decay of the 490 nm chromophore (Figure 4a and Figures S28−S32). At maximum accumulation of this visible chromophore, three major EPR-active species can be observed. There is a high-spin iron(III) species with signals in the $g = 9$ and 4−6 regions that account for ∼40% of total Fe; this species exhibits a time course that does not correlate at all with the kinetic behavior of **2**, suggesting that it is associated with side reactions often observed in this kind of chemistry. This high-spin iron(III) species can also be observed in the Mössbauer spectrum of the same sample (Figure S33) and represents ∼40% of the total Fe in the sample as well.

There are also two $S = 1/2$ species. The minor component, representing 5% of total Fe, exhibits g values at 2.20, 2.19, and 1.99 (**2a**, g_{max} = 2.20 species), and its simulated spectrum is shown in blue in Figure 4a. The major component, representing ∼40% of total Fe, has g-values at 2.07, 2.01, and 1.95 (**2b**, g_{max} = 2.07 species); its simulation is shown in red in Figure 4a. Significantly, the growth and decay of both EPR species closely track the time course of the 490 nm chromophore (Figure 4b). More importantly, addition of 50 equiv cyclohexane at −50 °C accelerated the decay of the 490 nm chromophore, in tandem with the decay of both **2a** and **2b**. Upon complete decay of the 490 nm chromophore, a new low-spin iron(III) center with g values at 2.21, 2.14, and 1.97 (labeled the g_{mid} = 2.14 species) was observed, which represents 28% of total Fe. However, its formation is not directly connected with the decay of the 490 nm chromophore either in the absence or the presence of cyclohexane (Table S6). The most important observation from this study is that both **2a** and **2b** are kinetically connected with the 490 nm chromophore and are therefore likely to be species that are in equilibrium with each other. (For more detailed discussion, see text associated with Table S6 and Figures S28−S32.)

At near maximal development of the 490 nm chromophore, the two isomeric $S = 1/2$ species in equilibrium with each other account for ∼45% of the Fe. If only the g_{max} = 2.20 species (**2a**) contributes to the 490 nm band, it would have an unreasonably large ε_{490} of 36 000 M^{-1}cm^{-1}, whereas a more reasonable ε_{490} ≈ 4500 M^{-1}cm^{-1} results if only the 2.07 species (**2b**) contributes to the absorption band. Clearly, **2b** must be associated with the 490 nm band, if not alone then in concert with **2a**. It is interesting to note that an ε_{490} ≈ 4000 M^{-1}cm^{-1} (assuming that both **2a** and **2b** contribute to the chromophore) would compare well with that of the 460 nm chromophore (ε_{460} ≈
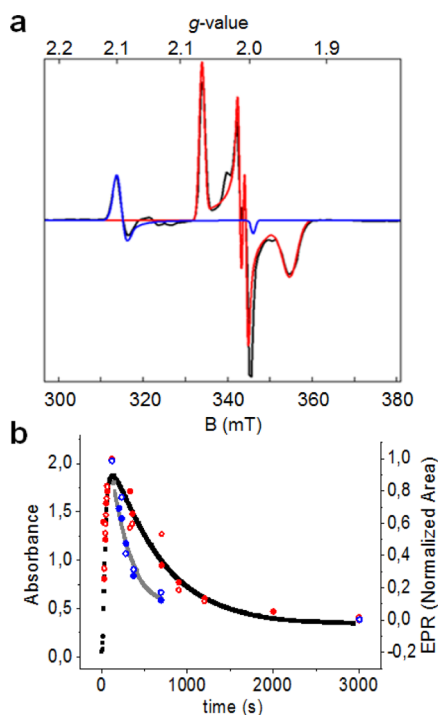
Figure 4. (A) X-band EPR spectrum of a 1 mM solution of **1** in 1:3 (v/v) acetonitrile/acetone reacted with 5 equiv AcOOH at −50 °C and frozen at t = 120 s. EPR conditions: T = 20 K, 0.2 mW microwave power, 1 mT modulation. Shown is the g = 2 region of the experimental spectrum (black). The theoretical curves (red and blue) are S = 1/2 SpinCount simulations. Blue: g_{max} = 2.20 species (**2a**) simulated with g = 2.20, 2.19, 1.99 (5% of Fe). Red: g_{max} = 2.07 species (**2b**) simulated with g = 2.07, 2.01, 1.95 (40% of Fe). The sharp feature at g = 2.00 belongs to an unknown minor species (<2%). Spectra along the time course that also include the low field region are shown in the Figures S28−S32. (B) Time course of **2** generated by adding 5 equiv AcOOH to a 1 mM solution of **1** in 1:3 (v/v) acetonitrile/acetone at −50 °C. Black squares: formation and self-decay of the 490 nm chromophore. Gray line shows the decay of the chromophore after the addition of cyclohexane (50 equiv) upon maximum formation of **2** (near 120 s). Red open and filled circles represent the respective amounts of the g_{max} = 2.20 and g_{max} = 2.07 species (**2a** and **2b**) during the formation and self-decay of the 490 chromophore. Blue open and filled circles respectively mark the time course of the g_{max} = 2.20 and 2.07 species (**2a** and **2b**) during the decay of **2** after the addition of 50 equiv of cyclohexane.

4000 $M^{-1}cm^{-1}$) recently found in the reaction of $[Fe^{II}(TPA*)]^{2+}$ with $H_2O_2/AcOH$ or AcOOH at −40 °C, which is associated with an S = 1/2 acylperoxoiron(III) intermediate $[Fe^{III}(OOAc)(TPA*)]^{2+}$ (**3**, TPA* = tris(3,5-dimethyl-4-methoxy-2-pyridylmethyl)amine), even though the latter has a much greater EPR anisotropy (g = 2.58, 2.38, 1.72).[40] It should also be noted that Talsi et al. have recently found a similar transient species in epoxidation reactions with the $[Fe(TPA*)]$ catalyst performed at −85 °C with g-values like those of the g_{max} = 2.07 species.[43] However, this species accumulates to only ∼1% of total Fe in the $[Fe(TPA*)]$ sample.

By analogy to the 460 nm chromophore **3** derived from the Fe(TPA*) catalyst, we first considered the assignment of the 490 nm intermediate **2** to a low-spin $[Fe^{III}(OOAc)-(PyNMe_3)]^{2+}$ complex. In previous work, we reported that the Mössbauer and EPR data of **3**, having g = (2.58, 2.38, 1.72), fit well to the Griffith−Taylor model, which generally describes

the g-values of low-spin Fe^{III} complexes quite well.[44,45] This model considers spin−orbit coupling within a T_{2g} set that is energetically well separated from the E_g set and low-lying charge transfer states. The assignment of **3** as a low-spin S = 1/2 acylperoxoiron(III) species was corroborated by resonance Raman and ESI−MS experiments.[40] To serve as an analog for the putative $[Fe^{III}(\kappa^2\text{-}OOAc)(PyNMe_3)]^{2+}$ species, the $[Fe^{III}(tBuCON(H)O)(PyNMe_3)]^{2+}$ complex (**4**) has been synthesized and structurally characterized, where a hydroxamate replaces the bidentate peracetate ligand (see SI for details). Complex **4** exhibits an axial EPR spectrum with g = 2.21 and 1.94 (Figure S25) that is similar to that of **2a**, suggesting that the latter arises from the $[Fe^{III}(\kappa^2\text{-}OOAc)-(PyNMe_3)]^{2+}$ complex.

In stark contrast, the g-values of **2b** do not fit to the Griffith−Taylor model. To obtain the observed g values would require T_{2g} splittings in excess of 10 000 cm^{-1}, and the resonance at g = 2.01 would be especially troublesome to fit.[44,45] While this argument does not necessarily rule out the possibility of **2b** as a low-spin Fe^{III} complex, the small spread of its g-values (2.07, 2.01, 1.95) would indicate a very unusual nonheme low-spin iron(III) center that has not yet been observed.[35] So, an alternative description needs to be considered.

Comparison of the g-values of **2b** with those reported for a handful of $Fe^V(O)(L)$[31,43,46,50] and $Fe^{IV}(O)(L^{\bullet+})$[52−54] species (where $L^{\bullet+}$ stands for a ligand radical cation) suggests a possible solution (Table 2). In particular, the g-values of **2b** and $[Fe^V(O)(NC(O)Me)(TMC)]^+$ **5** (g = 2.053, 2.010, 1.971), closely resemble each other.[46] Furthermore, both exhibit highly anisotropic ^{57}Fe A-tensors. Examination of the EPR spectrum of an ^{57}Fe-enriched sample of **2** revealed a large magnetic hyperfine interaction of 47 MHz at $g_{mid} = g_y$ = 2.01 and two much smaller components at g_{max} and g_{min} (see Figure S34). For comparison, the EPR spectrum of an ^{57}Fe-enriched sample of **5** also showed a large component of 47 MHz, but this was observed along the direction of $g_{max} = g_x$ = 2.05 (the unpaired electron of the Fe^V is in d_{yz}),[47] suggesting some (possibly significant) differences between **2b** and **5**. Nevertheless, these two complexes are clearly different from the S = 1/2 $Fe^{IV}(O)(L^{\bullet+})$ species such as Compound I of horseradish peroxidase, chloroperoxidase, and cytochrome P450 (Table 2),[48,49] which all have *axial* ^{57}Fe A-tensors with $|A_x| \approx |A_y| \gg A_z$. Both the d_{yz} and d_{xz} orbitals of the S = 1 $Fe^{IV}(O)$ complexes are singly occupied, in contrast to the S = 1/2 $Fe^V(O)$ centers, which have only one unpaired electron in either the d_{xz} or d_{yz} orbital (with d_{xy} doubly occupied). An x/y anisotropy is also observed for $[Fe^V(O)(TAML)]^-$, the first characterized example of a bona fide oxoiron(V) complex (Table 2).[50] We can thus safely conclude that **2b** cannot arise from an $Fe^{IV}(O)(L^{\bullet+})$ complex. However, the presence of a highly anisotropic ^{57}Fe A-tensor does not allow us to distinguish between an S = 1/2 peroxoiron(III) and an S = 1/2 oxoiron(V) center, as similar anisotropies of the ^{57}Fe A-tensor have been observed for some low-spin iron(III) complexes having g-values close to g = 2.0, such as the S = 1/2 $[Fe^{III}(\eta^1\text{-}OOH)(N4Py)]^{2+}$ complex (Table 2).[51]

At this point, our usual strategy would have been to carry out a complementary Mössbauer analysis in order to distinguish between an S = 1/2 peroxoiron(III) and an S = 1/2 oxoiron(V) center. However, our attempts to identify unique Mössbauer features associated with the g_{max}= 2.07 species (**2b**) were stymied by the spectral complexity of samples (Figure S33) that have at least four EPR-active species, all of which would be

Table 2. g- and A-values of Established and Proposed Fe^V(O)(L) and Fe^{IV}(O)(L$^{•+}$) Complexes and Related S = 1/2 Peroxoiron(III) Species

complex[a]	$g_{x,y,z}$	^{57}Fe A$_{x,y,z}$ (MHz)	ref
[Fe^V(O)(TAML)]$^-$	1.99, 1.97. 1.74	−67, −2, −22	50
[Fe^V(O)(bTAML)]$^-$	1.98, 1.94, 1.73		31
[Fe^V(O)(NC(O)Me)(TMC)]$^+$ (**5**)	2.05, 2.01, 1.97	−47, −17, 0	46
[Fe^V(O)(TPA*)]$^{3+b}$	2.07, 2.01, 1.96		43
[Fe^{IV}(O)(Cl-acac$^{•-}$)(Me$_3$TACN)]$^{2+c}$	1.97, 1.93, 1.91		52
[Fe^{IV}(O)(TBP$_8$Cz$^{•+}$)]	2.09, 2.05, 2.02		53
[Fe^{IV}(NTs)(TBP$_8$Cz$^{•+}$)]	2.1, 2.1, 2		54
HRP-Cpd I	1.99 (broad)	−26, −26, −8[d]	48
CPO-Cpd I	1.72, 1.61, 2.00	−42, −41, −3	49
CYP119-Cpd I	2.00, 1.96, 1.86	−38, −44, −4	49
[Fe^{III}(κ^2-OOAc)(TPA*)]$^{2+}$ (**3**)	2.58, 2.38, 1.72	−62, +26, +42	40
[Fe^{III}(η^1-OOH)(N4Py)]$^{2+}$	2.16, 2.11, 1.98	−9, −53, +6	51
2a	2.20, 2.19, 1.99	not determined	this work
2b	2.07, 2.01, 1.95	A$_x$ ≪ A$_y$ = 47 ≫ A$_z$	this work

[a]Abbreviations used: TAML = tetraamidate macrocyclic ligand, bTAML = biuret tetraamidate macrocyclic ligand, TMC = tetramethylcyclam, TPA* = tris(3,5-dimethyl-4-methoxy-pyridyl-2-methyl)amine, Me$_3$TACN = 1,4,7-trimethyl-1,4,7-triazacyclononane, Cl-acac =3-chloro-acetylacetonate, TBP$_8$Cz = octakis(4-*tert*-butylphenyl)corrolazine, HRP = horseradish peroxidase; CPO = chloroperoxidase, CYP119 = cytochrome P-450 from *Sulfolobus acidocaldarius*, N4Py = bis(2-pyridylmethyl)-bis(2-pyridyl)methylamine. [b]This species has the same g-values as **2b** but represents only ca. 1% of the iron in the sample. The iron(V) oxidation state proposed for this species has not been established. [c]The proposed formulation for this intermediate needs further spectroscopic corroboration. [d]Quoted for the local S = 1 Fe^{IV} site in a coupled system.

expected to exhibit Mössbauer spectra with magnetic hyperfine features even without an applied magnetic field (see SI for further comments). What emerges from our EPR studies is that **2b** must have an unusual electronic structure, either in an S = 1/2 iron(III) description with a small spread of g-values that has yet to be observed for a nonheme low-spin iron(III) center[35] or an S = 1/2 oxoiron(V) description for which there are only three well characterized examples for comparison, namely the TMC complex and the two TAML complexes listed in Table 2.

The insights derived from the EPR analysis must be interpreted within the context of the kinetic results, which show that **2a** and **2b** both rise and fall in concert with the 490 nm chromophore and are thus in equilibrium with each other. If **2b** is assigned to a low-spin iron(III) center with an unusual electronic structure, it would most likely be a geometric isomer of the acylperoxoiron(III) center associated with **2a**. Such a geometric isomer would presumably have the bidentate acylperoxo ligand bound trans to different N atoms of the supporting PyNMe$_3$ macrocycle. However, it is unlikely that such an equilibrium would be facile at −40 °C. Furthermore, the subsequent rate determining cleavage of the strong substrate C—H bond would have to be effected by an acylperoxoiron(III) center, which is thus far unprecedented. However, assignment of **2b** to an S = 1/2 Fe^V(O) center would make it an electromer of the acylperoxoiron(III) center associated with **2a** that would form by a reversible O—O bond cleavage step (Scheme 1). There is experimental precedent for such equilibria as well as DFT calculations showing that higher-valent electromers of acylperoxoiron(III)

species are energetically accessible (see subsequent sections for discussion of these topics). The proposed oxoiron(V) species that we favor for the assignment of the g_{max} = 2.07 species (**2b**) would certainly have the oxidative power required to cleave strong C—H bonds directly, as demonstrated in this paper for the 490 nm chromophore.

Mass Spectroscopic Insights into the Nature of 2. Additional experimental evidence has been obtained in solution at −40 °C, corroborating the formation of a Fe^V(O)(O$_2$CR) derivative that is in equilibrium with the acylperoxoiron(III) intermediate. High-resolution cryospray mass spectrometry (CSI−MS) experiments at −40 °C showed **2** to exhibit a major peak at m/z 528.0893 with an associated isotopic pattern fully consistent with its formulation as {Fe(OOAc)(PyNMe$_3$)]-(CF$_3$SO$_3$)}$^+$ (Figure 5a) or either of its higher-valent electromers. CD$_3$COOD was added into the **1**/AcOOH reaction mixture during the formation of **2** at −40 °C. This experiment resulted in the appearance of a new feature at m/z 531 (Figure 5b), indicating the substitution of the acetate (CH$_3$CO$_2$) by d$_3$-acetate (CD$_3$CO$_2$). Control experiments showed that CD$_3$CO$_2$D and AcOOH did not exchange under the reaction conditions (see SI), so there must be a pathway for the incorporation of labeled acetate into the primary mass peak associated with **2**. We propose carboxylate exchange with the Fe^V(O) electromer as representing the most facile pathway that rationalizes the observed deuterium incorporation into **2** from CD$_3$COOD.

Corroboration for carboxylate exchange with **2** was obtained by investigating the reactions of **1**/AcOOH with cyclooctene in the presence of CD$_3$COOD. In room temperature reactions with 20 equiv AcOOH and no added CD$_3$COOD, cyclooctene was converted to cyclooctene oxide as the major product (17 TON) and *cis*-2-acetoxycyclooctanol as the minor product (2 TON). The latter has been reported in cyclooctene oxidations catalyzed by Fe(TPA) and Fe(BPMCN) with H$_2$O$_2$ in the presence of AcOH[15,55,56] and was proposed to arise from a [3 + 2] cycloaddition of a fleeting Fe^V(O)(OAc) oxidant to the C=C bond of the olefin substrate. It should be noted that the

Scheme 1. Reversible O—O Bond Cleavage of Acylperoxoiron(III) Species 2a to Oxoiron(V) Species 2b

a

b
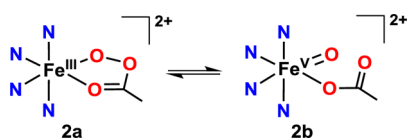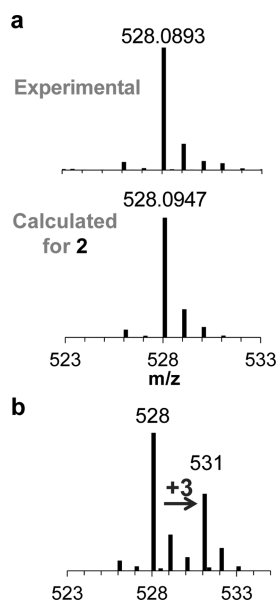
Figure 5. Cryospray mass spectral (CSI−MS) experiments. (a) Experimental and calculated patterns of **2** generated by reaction of **1** with 4 equiv peracetic acid in acetonitrile at −40 °C. (b) Spectrum of **2** generated with 4 equiv peracetic acid in the presence of 20 equiv acetic acid-d_4 at −40 °C. An M+3 ion was observed at m/z = 528, indicating that the CD_3CO_2 can be incorporated into this species. See Figures S35−S36 for full spectra.

exclusive *syn*-stereochemistry observed for the product is consistent with this scenario but not with a two-step mechanism involving initial epoxidation followed by epoxide ring opening. A control experiment in the absence of **1** afforded ∼5 times less epoxide product, but, importantly, there was no trace of *cis*-2-acetoxycyclooctanol. The *cis*-2-acetoxycyclooctanol product observed was 10% trideuterated in reactions of **1** and AcOOH with 200 equiv cyclooctene in the presence of 200 equiv CD₃COOD, both at −40 °C and at 25 °C, and also upon addition of 200 equiv CD₃COOD and 200 equiv cyclooctene after maximal formation of **2** at −40 °C, indicating that the acetate exchange in **2** occurs very fast (see Section VII of SI). Up to 29% of the labeled product was obtained after increasing the CD₃COOD amount to 500 equiv at 25 °C. These results clearly demonstrate that there must be a mechanism for the incorporation of deuterated acetate into the oxidant generated from **1** and AcOOH.

Comparison with Literature Precedents for Acylperoxoiron(III) Complexes. Intermediate **2** resembles in several respects the closely related low-spin acylperoxoiron-(III) intermediate **3** recently characterized at −40 °C in the reaction of Fe^{II}(TPA*) with H₂O₂/AcOH[40] but differs in others. Both **2** and **3** exhibit similarly intense visible chromophores in the 450−500 nm region that are associated with S = 1/2 EPR signals and undergo self-decay in MeCN at −40 °C with k_{obs} values of 0.02 s^{-1}. However, the reactivity of **2** significantly differs from that of **3**. Upon its generation, **3** persists in a steady state phase and undergoes rate-determining O—O bond cleavage that is substrate-independent. In contrast, **2** decays at a rate that depends on the nature of the substrate and its concentration, indicating that, unlike **3**, **2** directly reacts with alkanes. Moreover, the substrate-dependent decay of **2** is associated with two S = 1/2 species with g_{max} = 2.20 and 2.07 (**2a** and **2b**), respectively. These two species maintain a constant intensity ratio as **2** decays at different rates in the course of oxidizing various substrates. To accommodate these observations, we propose the possibility of a reversible O—O bond cleavage equilibrium between the [Fe^{III}(OOAc)-(PyNMe₃)]$^{2+}$ (**2a**, g_{max} = 2.20) and the highly oxidizing high-valent iron-oxo species [Fe^V(O)(OAc)(PyNMe₃)]$^{2+}$ (**2b**, g_{max} = 2.07) which acts as the actual oxidant (Scheme 2). Reversible cleavage of the O—O bond has in fact been demonstrated for a peroxocarbonatoiron(III) complex by Suzuki and co-workers, resulting in the incorporation of labeled water into the bound peroxocarbonate moiety and label scrambling.[57] It is highly unlikely that the observed incorporation of deuterated acetate into **2** occurs by direct exchange with the acylperoxoiron(III) species **2a**, but it could easily come about by ligand exchange of CD₃COOD with the Fe^V(O)(OAc) electromer **2b**. Our experimental results thus support the notion of energetically accessible higher-valent electromers in equilibrium with the acylperoxoiron(III) species, a notion first proposed by Shaik and co-workers based on DFT calculations on related systems.[17,40] The existence of this equilibrium allows **2** to attack strong C—H bonds directly and rapidly, a kinetic behavior that makes **2** unique among the few characterized first-row transition metal acylperoxo complexes reported so far including iron,[58,59] copper,[60−62] and nickel,[63] which are generally much more stable and sluggish in cleaving C—H bonds.

Comparison of the C—H Bond Cleavage Reactivities of 2 and Cpd I. In Figure 3, **2** was shown to be at least an order of magnitude faster with respect to HAT from cyclohexane than the most reactive nonheme iron-oxo complex

Scheme 2. Proposed Mechanism for the Reaction of 1/AcOOH with Substrates
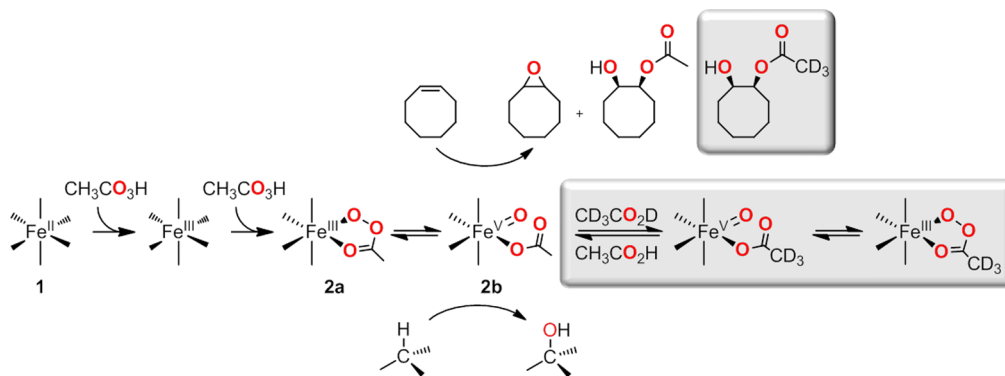
described to date. A comparison can be also made between **2** and Cpd I, the highly reactive oxoiron(IV) oxidant in heme chemistry. The second order rate constant (k_2) of 2.8 M^{-1} s^{-1} for the reaction of **2** with cyclohexane at 232 K is 25-fold faster than that measured for the Cpd I model $[Fe^{IV}(O)(TDCPP^\bullet)]^+$ (TDCPP = tetrakis(2,6-dichlorophenyl)porphyrin) at the same temperature.[33] However, the k_2 value for the reaction of **2** with toluene at 298 K of 6×10^3 M^{-1} s^{-1}, as estimated from the Eyring parameters obtained at lower temperature ($\Delta H^\ddagger = 27(1)$ kJ mol^{-1}, $\Delta S^\ddagger = -82(5)$ J K^{-1} mol^{-1}, Figure S19), is only 2 orders of magnitude smaller than the k_2 value for p-toluic acid oxidation recently determined by Groves for the highly reactive Cpd I intermediate of a heme-thiolate peroxygenase.[64] When the toluene oxidation rate of **2** is mapped onto a plot of log k_2 values of different oxidants toward toluene vs the strength of the O—H bond formed,[65] an estimate of ~101 kcal·mol^{-1} can be made for the FeO—H bond that forms in the HAT reaction by **2** (Figure S20), which is substantially larger than those determined for $Fe^{III}O(R)$ (~85 kcal·mol^{-1}) and heme $Fe^{IV}(O)$ oxidants (~90 kcal·mol^{-1})[66,67] and just 2 kcal·mol^{-1} smaller than the 103 kcal·mol^{-1} value associated with the heme-thiolate peroxygenase Cpd I.[64]

■ CONCLUSIONS

We have thus collected a set of spectroscopic and reactivity data on **2** that shed light on a remarkable oxidant **2** that is generated at −40 °C by the reaction of peracetic acid with the nonheme iron catalyst **1**. Oxidant **2** is an order of magnitude faster at cleaving the C—H bonds of cyclohexane than the most reactive nonheme oxoiron(IV) complexes reported thus far[33,34] and 4 orders of magnitude faster than oxoiron(V) TAML complexes at the same temperature.[30] Oxidant **2** is also capable of catalytic turnover, unlike the latter complexes, which at best can only carry out stoichiometric substrate oxidation. Furthermore, despite its high reactivity, **2** effects site-selective C—H bond functionalization that is responsive to electronic and steric parameters. Most significantly, in stark contrast to the reactivity of several nonheme oxoiron(IV) and oxoiron(V) complexes that can cleave strong C—H bonds but generate long-lived carbon-centered radicals,[28,29,31,68] **2** carries out C—H hydroxylations with high stereoretention. This observation is especially remarkable because structurally related iron complexes catalyze this challenging reaction with reactivity patterns analogous to those exhibited by **2**.[24,25,69] Selectivity in C—H bond reactivity converts them into very interesting tools for synthetic organic chemistry, yet the active species that account for this selectivity have not been directly observed. Therefore, this work constitutes the first case where the species responsible for stereospecific and site selective C—H hydroxylation with this class of catalysts is spectroscopically trapped, and its catalytic reactivity against C—H bonds could be directly demonstrated. Results presented here identify the major component of **2**, namely **2b**, as a species having unusual electronic structure. The g values of this $S = 1/2$ species exhibit a small g anisotropy that is not observed thus far for a nonheme low-spin iron(III) center but resembles that of a recently described oxoiron(V) complex **5**. We thus favor the latter formulation as a rationale for the unprecedentedly C—H bond cleavage reactivity found in the reaction of **1** with peracetic acid.

■ EXPERIMENTAL SECTION

Materials. Reagents and solvents used were of commercially available reagent quality, unless otherwise stated. Solvents were purchased from Scharlab, Acros, or Sigma-Aldrich and used without further purification. Peracetic acid was purchased from Aldrich as a 32 wt % solution in acetic acid containing less than 6% H_2O_2. Preparation and handling of air-sensitive materials were carried out in a N_2 drybox (Jacomex) with O_2 and H_2O concentrations <1 ppm. Synthesis of compound **1** is detailed in the SI.

Physical Methods. High resolution mass spectra (HR−MS) were recorded on a Bruker MicrOTOF-Q IITM instrument using ESI or Cryospray ionization sources at Serveis Tècnics of the University of Girona. Samples were introduced into the mass spectrometer ion source by direct infusion using a syringe pump and were externally calibrated using sodium formate. A cryospray attachment was used for CSI−MS (cryospray mass spectrometry). The temperature of the nebulizing and drying gases was set at −40 °C. The instrument was operated in positive ion mode. NMR experiments were performed on a Bruker Ultrashield Avance III400 and Ultrashield DPX300 spectrometers. UV−vis spectroscopy was performed with an Agilent 50 Scan (Varian) UV−vis spectrophotometer with 1 cm quartz cells. Low temperature control was achieved with a cryostat from Unisoku Scientific Instruments, Japan. GC product analyses were performed on an Agilent 7820A gas chromatograph equipped with an HP-5 capillary column 30m × 0.32 mm × 0.25 μm and a flame ionization detector. Stopped-flow experiments were carried out using an SFM4000 Biologic instrument provided with a cryo-stopped-flow accessory fitted to a Huber CC-905 bath.

Mössbauer spectra were recorded with two spectrometers, using Janis Research (Wilmington, MA) SuperVaritemp dewars that allow studies in applied magnetic fields up to 8.0 T in the temperature range from 1.5 to 200 K. Mössbauer spectral simulations were performed using the WMOSS software package (WEB Research, Minneapolis). Perpendicular (9.63 GHz) mode X-band EPR spectra were recorded on a Bruker EPP 300 spectrometer equipped with an Oxford ESR 910 liquid helium cryostat and an Oxford temperature controller. The quantification of the signals was relative to a Cu-EDTA spin standard. Software for EPR analysis was provided by Dr Michael P. Hendrich of Carnegie Mellon University.

Generation of 2. In a typical experiment, a 1 mM solution of **1** in dry acetonitrle was prepared inside the glovebox and 2 mL of this solution were placed in a UV−vis cuvette (2 μmols of **1**). The quartz cell was capped with a septum and taken out of the box, placed in the Unisoku cryostat of the UV−vis spectrophotometer and cooled down to 238 K. After reaching thermal equilibrium an UV−vis spectrum of the starting complex was recorded. Then, 50 μL of a solution containing 66 μL of 32% peracetic acid in 2 mL of dry acetonitrile were added (8 μmols). The formation of a band at λ_{max} = 490 nm and a shoulder at λ_{max} = 660 nm was observed. Compound **2** was fully formed after 70 s. In the reactions where the intermediate species is generated in acetone, a 4 mM solution of the complex in acetonitrile was prepared and then further diluted with the corresponding amount of dry acetone.

Kinetic Analysis of Reactions against Alkanes. The experiments were carried out by mixing thermostated acetonitrile solutions of **1** and peracetic acid (1:4 ratio) in a delay line. The resulting solution was aged for the time required to achieve the maximum concentration of **2**, and then it was mixed with a solution of the substrate. The concentration of the substrate in the observation cell was changed by using different ratios of the volumes in the second mixing. In any case, the substrate concentration was always in pseudo-first order excess with respect to **2**, and the kinetics of reaction was monitored by measuring the spectral changes with time using a diode-array detector. The data acquired after the second mixing were analyzed using the standard software of the stopped-flow instrument. In all cases, a satisfactory fit was obtained for the disappearance of **2** using a single exponential.

Analysis of the Oxidation Products. Once **2** was fully formed, 100 μL of a solution containing the corresponding equivalents of the desired substrate were added in the cuvette. The decay of the band at λ = 490 nm was monitored and after complete decay the cuvette was let to attain room temperature. Biphenyl was added as internal standard, and the iron complex was removed by passing the solution through a

short path of silica. The products were then eluted with ethyl acetate and then analyzed by GC.

Catalytic Experiments at Room Temperature with 1/AcOOH. In a typical experiment, 2 mL of a 1 mM solution of **1** in acetonitrile were placed in a 20 mL vial together with the appropriate amount of the desired substrate. Then, the corresponding amount of peracetic acid solution diluted in acetonitrile was added over 30 min. The solution was stirred for extra 15 min. For alkane oxidation, an internal standard (biphenyl) was added after the reaction was completed. The iron complex was removed by passing the solution through a short path of silica followed by elution with ethyl acetate (2 mL). Finally, the solution was subjected to GC analysis. For the oxidation of cyclooctene, the sample was treated with acetic anhydride (1 mL) together with 1-methylimidazole (0.1 mL), stirred for 15 min at r.t. to esterify the alcohol products. Then 3 mL of ice were added and stirred for 10 min. Biphenyl was added as an internal standard at that point, and then the organic products were extracted with $CHCl_3$ (2 mL). The organic layer was extracted and washed with H_2SO_4 (2 mL, 1M), saturated aq. $NaHSO_3$ (2 mL) and water (2 mL). The organic layer was dried over $MgSO_4$, filtered through a short path of diatomaceous earth and subjected to GC or GC−MS analysis.

■ ASSOCIATED CONTENT

Ⓢ Supporting Information

The Supporting Information is available free of charge on the ACS Publications website at DOI: 10.1021/jacs.5b09904.

> Experimental details for the preparation and characterization of ligand PyNMe3, and compounds **1**, **2′** and **4**; UV−vis stopped-flow experiments for the generation and reactivity of **2**; details on EPR and Mössbauer experiments; carboxylate exchange experiments of **2** with acetic acid-d_4 (PDF)
> X-ray data for **1** (CIF)
> X-ray data for **4** (CIF)

■ AUTHOR INFORMATION

Corresponding Authors
*manuel.basallote@uca.es
*emunck@cmu.edu
*larryque@umn.edu
*anna.company@udg.edu
*miquel.costas@udg.edu

Notes
The authors declare no competing financial interest.

■ ACKNOWLEDGMENTS

■ REFERENCES

(1) Dyker, G. *Handbook of C-H Transformations*; Wiley-VCH: Weinheim, 2005.

(2) Meunier, B.; de Visser, S. P.; Shaik, S. *Chem. Rev.* **2004**, *104*, 3947−3980.

(3) Montellano, P. R. O. d. *Cytochrome P450: Structure, Mechanism, and Biochemistry*; Springer: New York, 2005.

(4) Costas, M.; Mehn, M. P.; Jensen, M. P.; Que, L. *Chem. Rev.* **2004**, *104*, 939−986.

(5) Abu-Omar, M. M.; Loaiza, A.; Hontzeas, N. *Chem. Rev.* **2005**, *105*, 2227−2252.

(6) Kovaleva, E. G.; Lipscomb, J. D. *Nat. Chem. Biol.* **2008**, *4*, 186−193.

(7) Barry, S. M.; Challis, G. L. *ACS Catal.* **2013**, *3*, 2362−2370.

(8) Company, A.; Lloret-Fillol, J.; Costas, M. In *Comprehensive Inorganic Chemistry II*; Reedijk, J., Poeppelmeier, K., Eds.; Elsevier: Oxford, 2013; Vol. 3, pp 487−564.

(9) Park, M. J.; Lee, J.; Suh, Y.; Kim, J.; Nam, W. *J. Am. Chem. Soc.* **2006**, *128*, 2630−2634.

(10) Seo, M. S.; Kamachi, T.; Kouno, T.; Murata, K.; Park, M. J.; Yoshizawa, K.; Nam, W. *Angew. Chem., Int. Ed.* **2007**, *46*, 2291−2294.

(11) Cho, J.; Jeon, S.; Wilson, S. A.; Liu, L. V.; Kang, E. A.; Braymer, J. J.; Lim, M. H.; Hedman, B.; Hodgson, K. O.; Valentine, J. S.; Solomon, E. I.; Nam, W. *Nature* **2011**, *478*, 502−505.

(12) Thibon, A.; Jollet, V.; Ribal, C.; Sénéchal-David, K.; Billon, L.; Sorokin, A. B.; Banse, F. *Chem. - Eur. J.* **2012**, *18*, 2715−2724.

(13) Prat, I.; Company, A.; Corona, T.; Parella, T.; Ribas, X.; Costas, M. *Inorg. Chem.* **2013**, *52*, 9229−9244.

(14) Britovsek, G. J. P.; England, J.; White, A. J. P. *Inorg. Chem.* **2005**, *44*, 8125−8134.

(15) BPMEN = N,N′-dimethyl-N,N′-bis(2-pyridylmethyl)ethane-1,2-diamine; BPMCN = N,N′-dimethyl-N,N′-bis(2-pyridylmethyl)-trans-1,2-diaminocyclohexane; TPA = tris(2-pyridylmethyl)amine; PDP = N,N′-Bis(2-pyridylmethyl)-2,2′-bipyrrolidine; PyTACN = 1,4-Dimethyl-7-(2-pyridylmethyl)-1,4,7-triazacyclononane.

(16) Chen, K.; Que, L. *J. Am. Chem. Soc.* **2001**, *123*, 6327−6337.

(17) Wang, Y.; Janardanan, D.; Usharani, D.; Han, K.; Que, L., Jr.; Shaik, S. *ACS Catal.* **2013**, *3*, 1334−1341.

(18) Prat, I.; Mathieson, J. S.; Güell, M.; Ribas, X.; Luis, J. M.; Cronin, L.; Costas, M. *Nat. Chem.* **2011**, *3*, 788−793.

(19) Oloo, W. N.; Que, L. *Acc. Chem. Res.* **2015**, *48*, 2612−2621.

(20) Costas, M.; Chen, K.; Que, L. *Coord. Chem. Rev.* **2000**, *200*, 517−544.

(21) Even though the $BDE_{C−H}$ of CH_3CN (93 kcal·mol^{-1}) is lower than that of some of the hydrocarbon substrates used in this work (e.g., BDE_{C6H12} = 99.3 kcal·mol^{-1}), acetonitrile oxidation does not take place due to polar effects. See: Roberts, B. P. *Chem. Soc. Rev.* **1999**, *28*, 25.

(22) Gomez, L.; Canta, M.; Font, D.; Prat, I.; Ribas, X.; Costas, M. *J. Org. Chem.* **2013**, *78*, 1421−1433.

(23) Canta, M.; Font, D.; Gomez, L.; Ribas, X.; Costas, M. *Adv. Synth. Catal.* **2014**, *356*, 818−830.

(24) Chen, M. S.; White, M. C. *Science* **2007**, *318*, 783−787.

(25) Chen, M. S.; White, M. C. *Science* **2010**, *327*, 566−571.

(26) Oloo, W. N.; Que, L. In *Comprehensive Inorganic Chemistry II*; Reedijk, J., Poeppelmeier, K., Eds.; Elsevier: Oxford, 2013; Vol. 6, pp 763−778.

(27) Liu, L. V.; Hong, S.; Cho, J.; Nam, W.; Solomon, E. I. *J. Am. Chem. Soc.* **2013**, *135*, 3286−3299.

(28) Kaizer, J.; Klinker, E. J.; Oh, N. Y.; Rohde, J.-U.; Song, W. J.; Stubna, A.; Kim, J.; Münck, E.; Nam, W.; Que, L. *J. Am. Chem. Soc.* **2004**, *126*, 472−473.

(29) Company, A.; Prat, I.; Frisch, J. R.; Mas-Balleste, R.; Guell, M.; Juhasz, G.; Ribas, X.; Munck, E.; Luis, J. M.; Que, L.; Costas, M. *Chem. - Eur. J.* **2011**, *17*, 1622−1634.

(30) Kundu, S.; Thompson, J. V. K.; Shen, L. Q.; Mills, M. R.; Bominaar, E. L.; Ryabov, A. D.; Collins, T. J. *Chem. - Eur. J.* **2015**, *21*, 1803−1810.

(31) Ghosh, M.; Singh, K. K.; Panda, C.; Weitz, A.; Hendrich, M. P.; Collins, T. J.; Dhar, B. B.; Gupta, S. S. *J. Am. Chem. Soc.* **2014**, *136*, 9524−9527.

(32) Hong, S.; Wang, B.; Seo, M. S.; Lee, Y.-M.; Kim, M. J.; Kim, H. R.; Ogura, T.; Garcia-Serres, R.; Clémancey, M.; Latour, J.-M.; Nam, W. *Angew. Chem., Int. Ed.* **2014**, *53*, 6388−6392.

(33) Seo, M. S.; Kim, N. H.; Cho, K.-B.; So, J. E.; Park, S. K.; Clemancey, M.; Garcia-Serres, R.; Latour, J.-M.; Shaik, S.; Nam, W. *Chem. Sci.* **2011**, *2*, 1039−1045.

(34) Biswas, A. N.; Puri, M.; Meier, K. K.; Oloo, W. N.; Rohde, G. T.; Bominaar, E. L.; Münck, E.; Que, L. *J. Am. Chem. Soc.* **2015**, *137*, 2428−2431.

(35) Sastri, C. V.; Lee, J.; Oh, K.; Lee, Y. J.; Lee, J.; Jackson, T. A.; Ray, K.; Hirao, H.; Shin, W.; Halfen, J. A.; Kim, J.; Que, L.; Shaik, S.; Nam, W. *Proc. Natl. Acad. Sci. U. S. A.* **2007**, *104*, 19181−19186.

(36) Company, A.; Gómez, L.; Güell, M.; Ribas, X.; Luis, J. M.; Que, L.; Costas, M. *J. Am. Chem. Soc.* **2007**, *129*, 15766−15767.

(37) Hitomi, Y.; Arakawa, K.; Funabiki, T.; Kodera, M. *Angew. Chem., Int. Ed.* **2012**, *51*, 3448−3452.

(38) Makhlynets, O. V.; Oloo, W. N.; Moroz, Y. S.; Belaya, I. G.; Palluccio, T. D.; Filatov, A. S.; Muller, P.; Cranswick, M. A.; Que, L.; Rybak-Akimova, E. V. *Chem. Commun.* **2014**, *50*, 645−648.

(39) Oloo, W. N.; Fielding, A. J.; Que, L. *J. Am. Chem. Soc.* **2013**, *135*, 6438−6441.

(40) Oloo, W. N.; Meier, K. K.; Wang, Y.; Shaik, S.; Munck, E.; Que, L. *Nat. Commun.* **2014**, *5*, 4041−4049.

(41) Makhlynets, O. V.; Rybak-Akimova, E. V. *Chem. - Eur. J.* **2010**, *16*, 13995−14006.

(42) The EPR of **2** in MeCN shows broad signals and it is difficult to integrate. Thus, **2** was generated in the glassy 1:3 MeCN/acetone solvent mixture to afford dramatically sharpened EPR signals.

(43) Lyakin, O. Y.; Zima, A. M.; Samsonenko, D. G.; Bryliakov, K. P.; Talsi, E. P. *ACS Catal.* **2015**, *5*, 2702−2707.

(44) McGarvey, B. R. *Coord. Chem. Rev.* **1998**, *170*, 75−92.

(45) Taylor, C. P. S. *Biochim. Biophys. Acta, Protein Struct.* **1977**, *491*, 137−148.

(46) Van Heuvelen, K. M.; Fiedler, A. T.; Shan, X.; De Hont, R. F.; Meier, K. K.; Bominaar, E. L.; Münck, E.; Que, J. L. *Proc. Natl. Acad. Sci. U. S. A.* **2012**, *109*, 11933−11938.

(47) For the extreme octahedral case, for which the tetragonal and rhombic distortions are small compared to the spin-orbit coupling constant ($\lambda \approx 380$ cm^{-1}), the *g*-values are close to *g* = 2.00; see for instance Figure 3 in Telser, J. *J. Braz. Chem. Soc.* **2006**, *17*, 1501−1515 for $A^2 \approx 1/3$. This, perhaps unlikely, case would be recognizable by Mössbauer spectroscopy, as the ^{57}Fe magnetic hyperfine tensor would differ considerably from that observed for the other region for which the *g*-values are close to *g* = 2, namely when the tetragonal distortion is large compared to λ..

(48) Schulz, C. E.; Rutter, R.; Sage, J. T.; Debrunner, P. G.; Hager, L. P. *Biochemistry* **1984**, *23*, 4743−4754.

(49) Rittle, J.; Green, M. T. *Science* **2010**, *330*, 933−937.

(50) de Oliveira, F. T.; Chanda, A.; Banerjee, D.; Shan, X.; Mondal, S.; Que, L.; Bominaar, E. L.; Münck, E.; Collins, T. J. *Science* **2007**, *315*, 835−838.

(51) Roelfes, G.; Vrajmasu, V.; Chen, K.; Ho, R. Y. N.; Rohde, J.-U.; Zondervan, C.; la Crois, R. M.; Schudde, E. P.; Lutz, M.; Spek, A. L.; Hage, R.; Feringa, B. L.; Münck, E.; Que, L. *Inorg. Chem.* **2003**, *42*, 2639−2653.

(52) Tse, C.-W.; Chow, T. W.-S.; Guo, Z.; Lee, H. K.; Huang, J.-S.; Che, C.-M. *Angew. Chem., Int. Ed.* **2014**, *53*, 798−803.

(53) McGown, A. J.; Kerber, W. D.; Fujii, H.; Goldberg, D. P. *J. Am. Chem. Soc.* **2009**, *131*, 8040−8048.

(54) Leeladee, P.; Jameson, G. N. L.; Siegler, M. A.; Kumar, D.; de Visser, S. P.; Goldberg, D. P. *Inorg. Chem.* **2013**, *52*, 4668−4682.

(55) Mas-Balleste, R.; Fujita, M.; Que, L., Jr. *Dalton Trans.* **2008**, 1828−1830.

(56) Iyer, S. R.; Javadi, M. M.; Feng, Y.; Hyun, M. Y.; Oloo, W. N.; Kim, C.; Que, L. *Chem. Commun.* **2014**, *50*, 13777−13780.

(57) Furutachi, H.; Hashimoto, K.; Nagatomo, S.; Endo, T.; Fujinami, S.; Watanabe, Y.; Kitagawa, T.; Suzuki, M. *J. Am. Chem. Soc.* **2005**, *127*, 4550−4551.

(58) Zhang, X.; Furutachi, H.; Tojo, T.; Tsugawa, T.; Fujinami, S.; Sakurai, T.; Suzuki, M. *Chem. Lett.* **2011**, *40*, 515−517.

(59) Khusnutdinova, J. R.; Luo, J.; Rath, N. P.; Mirica, L. M. *Inorg. Chem.* **2013**, *52*, 3920−3932.

(60) Ghosh, P.; Tyeklar, Z.; Karlin, K. D.; Jacobson, R. R.; Zubieta, J. *J. Am. Chem. Soc.* **1987**, *109*, 6889−6891.

(61) Sanyal, I.; Ghosh, P.; Karlin, K. D. *Inorg. Chem.* **1995**, *34*, 3050−3056.

(62) Kitajima, N.; Fujisawa, K.; Moro-oka, Y. *Inorg. Chem.* **1990**, *29*, 357−358.

(63) Nakazawa, J.; Terada, S.; Yamada, M.; Hikichi, S. *J. Am. Chem. Soc.* **2013**, *135*, 6010−6013.

(64) Wang, X.; Peter, S.; Kinne, M.; Hofrichter, M.; Groves, J. T. *J. Am. Chem. Soc.* **2012**, *134*, 12897−12900.

(65) Mayer, J. M. *Acc. Chem. Res.* **1998**, *31*, 441−450.

(66) Wolak, M.; van Eldik, R. *Chem. - Eur. J.* **2007**, *13*, 4873−4883.

(67) Groves, J. T.; Gross, Z.; Stern, M. K. *Inorg. Chem.* **1994**, *33*, 5065−5072.

(68) Kwon, E.; Cho, K.-B.; Hong, S.; Nam, W. *Chem. Commun.* **2014**, *50*, 5572−5575.

(69) Gómez, L.; Garcia-Bosch, I.; Company, A.; Benet-Buchholz, J.; Polo, A.; Sala, X.; Ribas, X.; Costas, M. *Angew. Chem., Int. Ed.* **2009**, *48*, 5720−5723.